www.revistageintec.net
ISSN: 2237-0722
revista GEINTEC Gestão, Inovação e Tecnologias

Electric Field Stress Control on FGM Spacer with Particle in a Three-Phase GIS Using Metal Inserts for Sustainable Agriculture

Yogesh Sambhana[1]; Sravana Kumar Bali[2]; V.S. Polamraju. Sobhan[3]; G.V. Nagesh Kumar[4]
[1]Vignan's Institute of Information Technology, Visakhapatnam.
[1]yogesh.sambhana@gmail.com
[2]Gitam Deemed to beUniversity, Visakhapatnam.
[2]sravanbali@gmail.com
[3]VFSTR Deemed to be University, Vadlamudi.
[3]pvssobhan@gmail.com
[4]JNTU, Pulivendula.
[4]drgvnk14@gmail.com

Abstract
Recently, this kind of agriculture is in danger of threatening its future since it depends upon industrial agriculture to provide the bulk of the food we eat. In high-voltage applications, the three-phase Gas Insulated Busductor (GIB) is considered to be the most important to fulfill high demand. Due to numerous flaws like as delamination, protrusion, etc. induced during the switching process, GIB is shown to have insulator failures. Those flaws have a significant impact upon the distribution of the electric field across the distance and hence on the entire GIB system, which causes enormous economic losses. This paper provides a post-type spacer for a three-phase GIB of delamination with a Functionally Degraded Material (FGM), an additional particle introduced at high voltage for the analysis of the adverse behavior of the spacer and subsequent insertion of metal inserts minimize the stress of the electronic field. By doping it with varying permittivity values to provide uniform electric field stress using a Finite element procedure, FGM is spatially dispersed with various filling materials. Simulation with planned spacer is performed as faults at various voltages and FGM grades with delamination and particle. With the insertion of the metal insert in the FGM spacer type postal insert, the influence of aluminum particles with varying delamination sizes is reduced and the findings obtained are given.

Key-words: Gas Insulated Busductor (GIB), Functionally Degraded Material (FGM), Electric Field.

1. Introduction

Whilst industrialized agriculture has succeeded in generating enormous amounts of food in the present day, due to agricultural issues the future of food production is at risk. The loss of farm land and the reduction in crop and livestock production are two of the most important challenges in agriculture. Gas Insulated Busduct (GIB) is wield in applications of large voltages because it serves important loads which are required for the satisfaction of high demand for electricity and public safety. The substations are ideally built to prevent natural disasters, such as environmental changes, inundations and so on. Although GIB is efficient than standard substations, they suffer few problems mostly due to spacer failures. Due to various flaws such as parcel contamination, protrusion, vacuum, depression, delamination etc., the isolating spacers lose their dielectric strength and therefore a proper technique for reducing electrical stress in the field must be applied.

Several researchers [2,3] have identified alternative to spacer design approaches, which can increase the reliability of GIS isolators by use of aluminum oxide (Al2O3) along with epoxy materials with functionally grading M, in literature, in order to study electric field stress in GIB and UHVAC gas isolated lines that play a vital role in the optimal allocation of energy. However, before they are applied in industry, there are further problems for manufacturing, design and the evaluation of FGM performance.With the use of centrifugal forces, few modes of growing and reducing can be achieved; a flexible manufacturing technique for FGM insulators is needed. It is found that the main source of electron emission was TJ, and found that the field stress was decreased by adding metal inserts to the interlocker with multifault flaws. Many investigated that the GIS compactness, electric field stress reduction technique is utilised to grade the plain epoxy length by using FEM analysis to varied permittivity values.The surface flashover in a cone-type spacer for GIS was examined in [6]. It was shown that it may be lowered by either a FGM spacer by putting the metal inserts at the triple point intersection; GIB. Several authors found that the failure of Spacer is one of the causes of the breakdown in dielectric power that generates surface flashing in GIS []. However, on the spacer surface there are numerous additional flaws like as delamination, fractures, particles, vacuums etc. However, this negative impact leads to GIB failure, and must thus be managed. It is observed that the voltage-time disruption of epoxy isolators including three micro-defect types (cracker, void, delamination, metal particles) was investigated and found that the apparent PD for GIS spacers is almost equal to 1 PC while those effects can be reduced by the use of metal inserts. Several researchers[10,11] have observed that ultrahigh-frequency (UHF) partial dissipation is the primary

reason for GIS failure caused by a number of defects and diversified optical sensing methods developed over the last couple of years because of highly sensitive and anti-electromagnetic interference that can be addressed through employees UHF external measuring system of the antenna sensor together with various techniques to gather PD signals from the GIS equipment. Jagadeesh Adari et.al[12] investigated how a cone type spacer may achieve fields within allowable values by utilizing three various types of FGM GIS methods, nevertheless, a post type GIB spacer can be extended. However, by adopting a new approach, i.e. by placing Metal Insert on the necessary place, the impact of the particle may be minimized. The dielectrical properties of the metallic particle in the type cone spacer were evaluated [21], which was better than disc type in the suggested FGM grading. The study can be done for FGM postal systems but, with metal inserts the spacing can be decreased.

The purpose of this work is to examine the E F Stress at TJ close to the box end in the 3-ϕ Gas Isolated Busduct with a FGM post interval of various types of grading. For electrical field stress at the enclosure end near the FGM spacer TJ, the insulation properties have been studied. The distribution of the Electrical Field Stress created by delaminating the FGM post-type intersection at the threefold junction is calculated. The EF stress in the triple junction of the cage end is analyzed, and the worsening of this stress can be reduced by inserting a recessed metal at the end of the cable with both faults together, for three different ranges of permissiveness values, types of FGM grades in TJ Y conductor, and for those two faults.

2. Modelling of 3- Phase GIB

Many scientists used two primary electronic equations, that is, the Laplace equation and Poisson equation with the limits of the supposed domain, to compute the electric field. These analytical or numerical procedures are solved using two ways. Three-phase GIB operates on high voltages, thus it is very difficult to analyze the equation of Laplace and the Poisson equation. Therefore, numerical approaches are employed in electrical field calculation to reduce this issue. The techniques are divided into the FDM, the FEM, the Charge Simulation Method (CSM) and the Border Elements Method (BEM). Although the preceding approaches have advantages and limitations, FEM is more adequate for tackling complicated questions. The electric field intensity "E" may be measured in a GIB tri-phase utilizing Poison Equation with the border condition of both spacer electrodes.

$$\vec{E} = -\nabla V \tag{1}$$

where, V is the capacity on the volt spacer.

From divergence theorem

$$\nabla.\vec{D} = \rho_v \tag{2}$$

The connection between the density of the flux and the intensity of the electrical field is described by,

$$\vec{D} = \varepsilon\vec{E} \tag{3}$$

where $\varepsilon = \varepsilon_o \varepsilon_r$ is insulating material permittivity.

Substituting equ (3) and equation (1) in equation (2),

$$\nabla.\varepsilon\vec{E} = \rho_v \tag{4}$$

$$\text{then , } \quad \nabla.\varepsilon(-\nabla V) = \rho_v \tag{5}$$

The equation (5) is reduced into the equation of Poisson by equation,

$$\nabla^2 V = \frac{-\rho_v}{\varepsilon} \tag{6}$$

When the load is supposed to be evenly distributed, the volume load density is zero, and so Equation (6) may be reduced as an equation of Laplace (7)

$$\nabla^2 V = 0 \tag{7}$$

So, the boundaris of the HV conductors in 3-ph GIB and the ground enclosure are represented in Figure 1 with the specifications as follows: The applied potential, at the HV Conductor at three ranges are, V_R(rms) = 72.5KV,132KV,220KV and Potential of Enclosure = 0V

Fig. 1 - Boundary Conditions 3-ϕ GIB

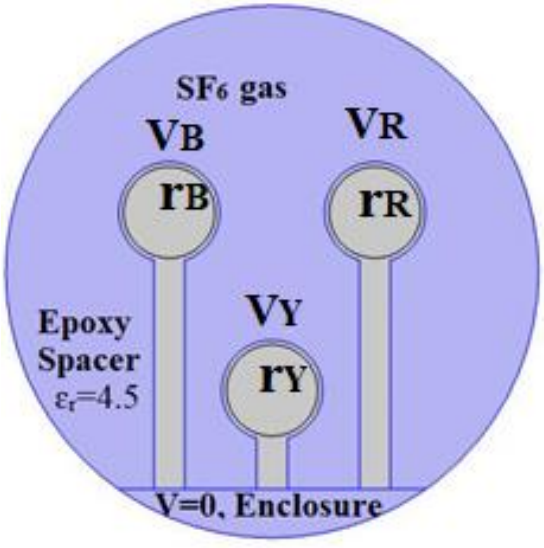

Consider, V_R , V_Y & V_B are the voltages at the three conductors R,Y,B w.r.t. ground at V=0 volts, and let r_R, r_Y, r_B, r are the radius of each conductor and ρ_R, ρ_Y, ρ_B are their line charge densities. For a 3-ϕ GIB with three equidistant conductors, the voltage is given by

$$V = \left[\frac{\rho_{RY}}{6\pi\varepsilon_O} \left(\ln \frac{d_{RY} d_{YB} d_{BR}}{r^3} \right) + \frac{\rho_{YB}}{6\pi\varepsilon_O} \left(\ln \frac{d_{RY} d_{YB} d_{BR}}{r^3} \right) + \frac{\rho_{BR}}{6\pi\varepsilon_O} \left(\ln \frac{d_{RY} d_{YB} d_{BR}}{r^3} \right) \right] \quad (8)$$

let $d_{RY} = d_{YB} = d_{BR} = d$,

where d_{RY}, d_{YB} and d_{BR} are the distance between each conductor in a 3-ϕ GIB.

$$\nabla^2 V = \nabla^2 \left\{ \left(\frac{\ln \frac{d}{r}}{2\pi\varepsilon_O} \right) \left[\rho_{RY} + \rho_{YB} + \rho_{BR} \right] \right\} = 0 \quad (9)$$

The electrical field intensity for a 3-ϕsystem is obtained from the FEM analytical idea

$$\vec{E} = \frac{\partial V}{\partial x} \vec{i} + \frac{\partial V}{\partial y} \vec{j} \quad (10)$$

$$\vec{E} = -\frac{1}{6\pi\varepsilon_O} \left\{ \frac{\partial}{\partial x} \left(\ln \frac{d_{RY} d_{YB} d_{BR}}{r^3} \left[\rho_{RY} + \rho_{YB} + \rho_{BR} \right] \right) \vec{i} + \frac{\partial}{\partial y} \left(\ln \frac{d_{RY} d_{YB} d_{BR}}{r^3} \left[\rho_{RY} + \rho_{YB} + \rho_{BR} \right] \right) \vec{j} \right\} \quad (11)$$

By utilizing FEM analysis, the energy stored in the full volume 'v' of the area, under continuous electro statics of constant dialectic strength (12).

$$W = \frac{1}{2} \int\int\int \varepsilon \left(\nabla^2 V \right) dv \quad (12)$$

In addition, the dielectric material is assumed an isotropic and the potential distribution does not vary in direction z, therefore the consideration is taken of a two dimensional Cartesian system. Hence In this comparable region, the total stored energy is provided by equation (18) which may be expressed from the equation (12).

$$W = \frac{1}{2} \iiint \left(\varepsilon_x \frac{\partial^2 V}{\partial x^2} + \varepsilon_y \frac{\partial^2 V}{\partial y^2} \right) dv \quad (13)$$

The energy density for a small area (dxdy) is given by

$$\frac{W}{z} = \frac{1}{2} \int\int \left(\varepsilon_x \frac{\partial^2 V}{\partial x^2} + \varepsilon_y \frac{\partial^2 V}{\partial y^2} \right) dx dy \quad (14)$$

where ε_x and ε_y are the dielectric constants in the respective parameters of x, y. By substituting Laplace's Equation in equation (12), the equation is simplified to

$$dW = \frac{1}{2}\int\int \varepsilon\left(\nabla^2 V\right)dxdy = 0 \qquad (15)$$

$$\boldsymbol{dW = O} \qquad (16)$$

Hence from the equation (16), the change in electrostatic energy stored is zero as the potential difference is constant inside the studied domain.

$$dW = \frac{\partial W}{\partial V_1}dV_1 + \frac{\partial W}{\partial V_2}dV_2 + ... + \frac{\partial W}{\partial V_n}dV_n = 0 \qquad (17)$$

The above equation (14) can be written as below

$$\left[\frac{\partial W}{\partial V_1} ..... \frac{\partial W}{\partial V_n}\right]\begin{bmatrix} dV_1 \\ ..... \\ ..... \\ dV_m \end{bmatrix} = 0 \qquad (18)$$

where ‘n’ and ‘m’ are number of unknown potential nodes and triangles considered in mesh of a three phase GIB.

To reduce electrostatic energy function, the parameters of $\frac{dW}{dV}$ must be equal to zero.

$$\text{i.e. } \left[\frac{\partial W}{\partial V_1} ..... \frac{\partial W}{\partial V_n}\right] = 0 \qquad (19)$$

3. Functionally Graded Material Post Type Spacer

A novel approach for the creation of a post-type distance in the 3-ϕ GIB proposal is the functional classification of materials to produce a unitary field distribution over its length. The FGM-Post type spacers are graded using several techniques, such as |-FGM, ⁻-FGM, (diagram/-)-FGM and the method of change of frequency, {i.e.} In this article the author of three sorts of degree, like GL-FGM, GH-FGM & GU-FGM, is picked out of all the aforementioned techniques. Centrifugal casting and 3D printing can be used to produce the FGM. 3D-Printing is a new technology involving the production process at the bottom. The following layers or parts of material are collected to produce 3D objects in computer control, whereas in Centrifugal casting the technique is applied from top to bottom. Figure 2 shows the manufacture of GL- FGM. In this article, for the three forms of classification, three alternative permittivity ranges are studied as follows. The FGM grading

categories with allowability values of various situations from Table 1. For the Table, for the permittivity fluctuation of example 1 for various FGM gradings is illustrated in Figure 3.

Fig. 2. Flow chart of fabrication of GL-FGM

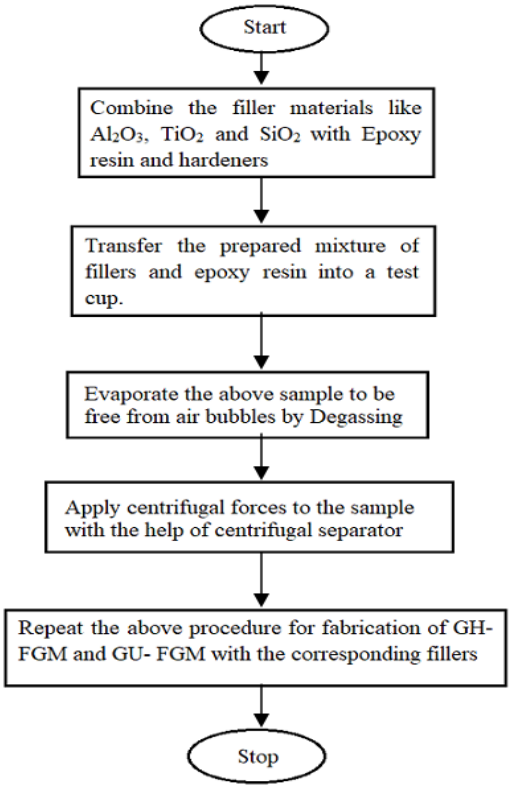

Table 1 - Permittivity Values of Gradings

Grading Type	Permittivity Ranges		
	Case1	Case 2	Case 3
GL-FGM	3.950 - 3.50	4.050 - 3.60	4.150 - 3.70
GH-FGM	3.50 - 3.950	3.60 - 4.050	3.70 - 4.150
GU-FGM	3.950 -3.50 - 3.950	4.050 - 3.60 - 4.050	4.150 - 3.70 - 4.150

Fig. 3 - Permittivity Variation of Gradings for Case 1

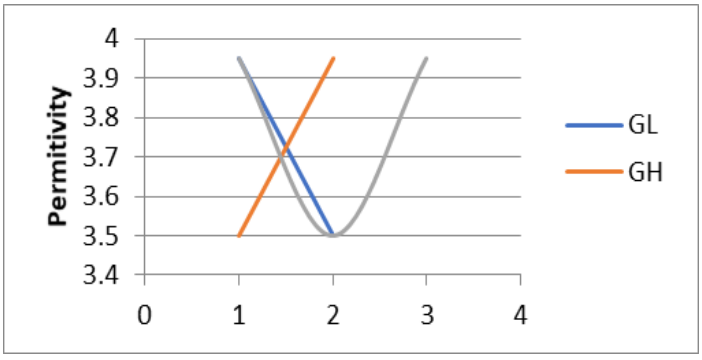

The FGM spacer is constructed with 10 identical grades of the same height and breadth of the three conductors. The grading takes place in three types of FGM method with various permittivity ranges

4. Delamination Impact on FGM Post Type Spacer

Delamination is one of the primary spacer defects that generates a distance between the spacers and the ends of the enclosure that is produced owing to unanticipated internal or external pressures such as mechanical stress, thermal stress and vibration during the GIB operating process. Delamination occurs as the most severe fault in the FGM after the distance between a three-stage gas insulated bus pipeline. The Electric Field the stress of the spacer is calculated on a GIB three-phase spacer (FGM Post type spacer) with dimensions D_w = 1.950 mm, D_h = 0.50 mm, G_w = 4.30 mm.

Fig. 4 - Representation of Delamination on Conductor Y

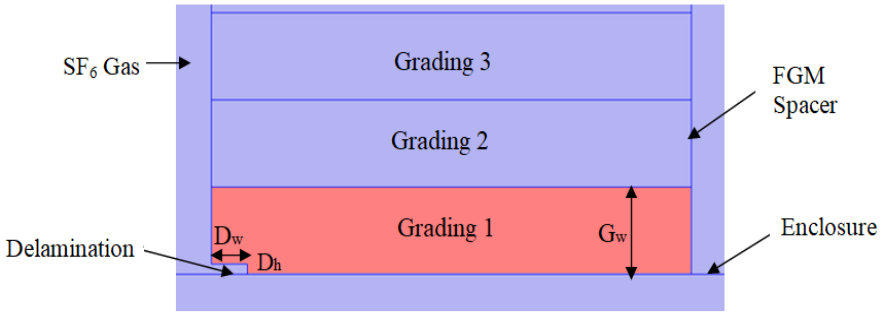

5. Effect of Particle adhering to FGM Post Type Spacer

Another important flaw in GIB's operation is the existence of metallic particles. During the production process, particles are generally generated by switching other switch disconnectors from circuit breakers or mechanic vibrations from heat. Particles generally come in many forms, such as spherical, elliptical or filamentary in various sizes. Most of these particles are detected within the box, on the conductor, or on the distance between the gaseous bus conduit. The presence of leading particles has a greater influence on the FGM than isolating particles because isolating particles don't lower collapse voltage if they just gain a charge and, as a result, larger particles have a greater effect than smaller particles. The electric field stress in the spacer must be calculated to understand the behaviour of the particles on the FGM post-spacer. As free particles are most hazardous compared to moving particles, free particles are taken as indicated in figure 5 for study of the FGM Post type

spacer in a GIB 3-ϕ. Here the particle is produced near the Driver Y TJ as compared to Driver R and Driver B it develops an electrical field stress. From the previous explanation, as the particle may have different materials, an investigation of three particles such as aluminum, copper and silver is carried out. The "Al" particle is seen to produce more electrical stress than the other two materials. The elliptical "Al" particle is regarded as 4mm wide with a circular edge radius of 8mm in height and 2mm round.

Fig. 5 - Particle Clinging to the FGM Spacer in the GIB

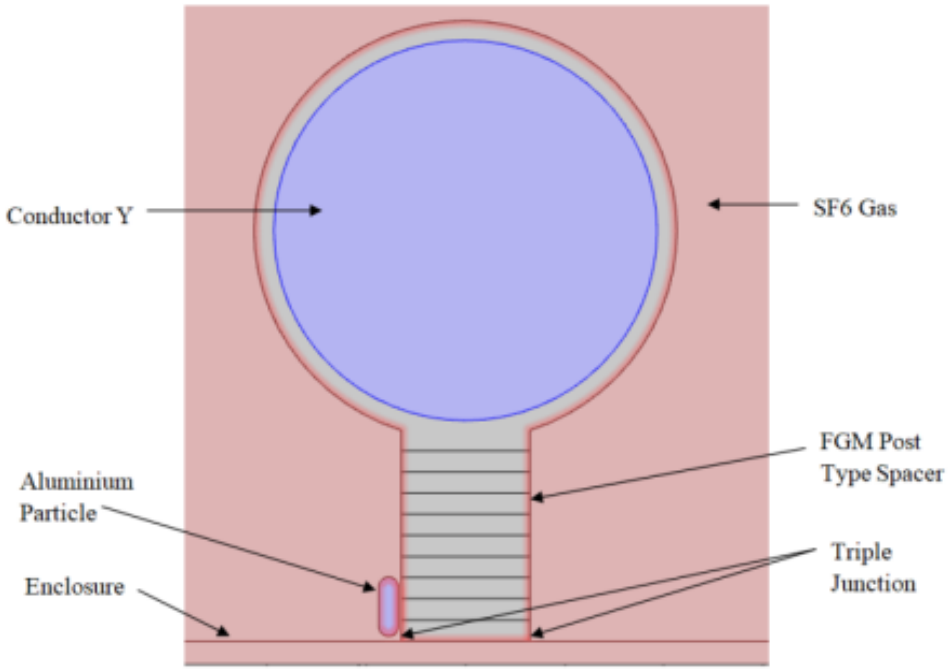

6. Results and Discussions

The fundamental modeling of a 3-ϕ GIB with a 225.50mm radius of the shared enclosure bus duct without delamination. The 3-ϕ GIB has a relatively primitive capacity of 1.00150 for SF6 gas. All three R, Y and B conductors are inside the same enclosure and positioned on the corners of a 38.660 mm equilateral triangle. The distance between driver R and the end of a box is 193.80 mm. The spacing distances are assumed as 43 mm and 193.80 mm from conductors Y to the of enclosure end, and the width of each spacer as 26 mm. FEM using epoxy/alumina composite as a spacer and three conductive systems located at the equidistance between each other, shielding the ball, the shielding ring and SF6 is a simulation of the 3-ϕ model in Figure 6.

Fig. 6 - Design Model of Three Phase GIB in 3D Cartesian System

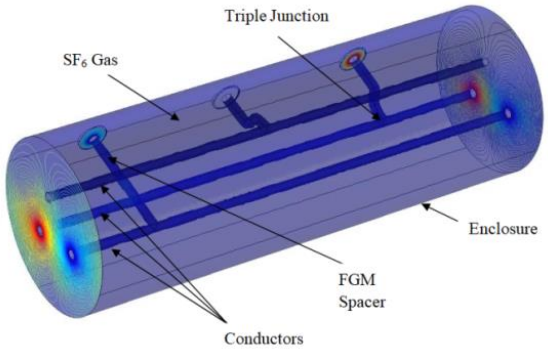

All the three R, Y & B conductors are positioned within the shared enclosed GIB at an equidistance from each other in the suggested simulation model. The Dirigent R is applied to RMS voltages of 72.5 kV, 132 k V and 220 kV, and with phase shift of -120^0& to $+120^0$, respectively, the voltages of the Dirigent VY & VB. The external electrode is zero voltage, i.e. the end of the box. The corresponding maximum voltages of driver R, Y, B are presented in Table 2 for these RMS voltages. The three-phase GIB has a relatively permittive capacity of 1.00150 for SF6 gas.

Table 2 - Maximum Voltages of Conductor R,Y,B

RMS Voltage (kV)	**$V_{R\ max}$ (kV)**	**$V_{Y\ max}$ (kV)**	**$V_{B\ max}$ (kV)**
V_1= 72.50	102.5150	-51.2580	-51.2580
V_2= 132.00	186.650	-93.3240	-93.3240
V_3= 220.00	311.080	-155.540	-155.540

Table 3 - Different Widths, Heights of Delamination

Width(mm)	**Height(mm)**	**V_1=72.5KV**	**V_2=132KV**	**V_3=200KV**
1.95 mm	1.46	0.129	0.234	0.391
	1	0.135	0.247	0.411
	0.5	**0.149**	**0.271**	**0.453**
1 mm	1.46	0.1205	0.219	0.365
	1	0.124	0.225	0.376
	0.5	0.136	0.248	0.413
0.5 mm	1.46	0.112	0.203	0.339
	1	0.116	0.211	0.352
	0.5	0.124	0.225	0.375

From table 3, Electrical field stress decreases by 1.950 mm, 1 mm & 0.50 mm, with a height reduction i.e. by 1.460 mm, 1.00mm & 0.50 mm, while the electrical field stress decreases. The width

(Dw) of 1.950 mm and height (Dh) of 0.50 mm, which is the greatest electric field stress. Therefore, for further study of the spacers in this three-phased GIB design this dimension (1.950mm X 0.50mm) has been shown in figure 6.

Table 4 represents, TJ's simulated electrical field stress results vary along with Al, Cu and Ag particles, along with delamination at varied operating voltage, with different types of particles. Table 4 shows that, compared with Cu and Ag, the electric field stress in all operating voltages for the particle formed of Al is large. Therefore, for further study of the spacers in that triphasic GIB design as seen in figure 7, the Al-particle with the above-mentioned delamination dimension is chosen.

Table 4 - Difference of Particles Together with Delamination Due to Electrical Field Stress

Type of Particle	**72.50kV**	**132.0kV**	**220.0kV**
Al	1.62310	0.29440	0.49110
Cu	1.622650	0.293980	0.490650
Ag	1.622550	0.29390	0.490550

Figure 7 shows 3-ϕ GIB design charts using the prior delamination dimensions and the FGM post type particle with MI. A metal insert (MI) with multiple shapes and dimensions and a corresponding MI with the form (i.e. the blending of rectangles and elliptic) with the dimensions of the rectangle as wide and height (22 mm X 1.50 mm) and ellipse with the length of the axis and b axis of (12.50 mm X 1.50 mm) was observed to help reduce the effect from delamination and the particular impact of FGM spacers.

Fig. 7 - FGM Post-type Spacer with Microdefect Delamination and MI

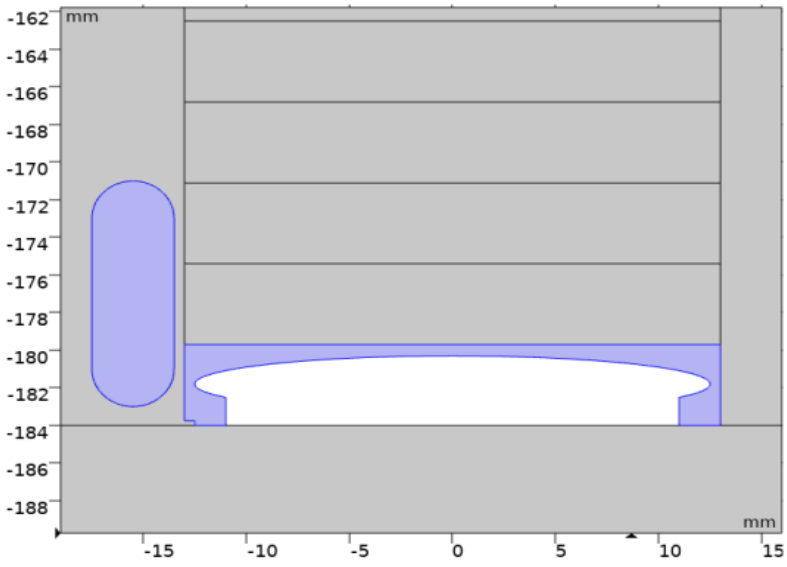

For above FGM Post type spacer with delamination led to a large electric field stress at TJ at the end of conductor Y, as seen in Figure 8, thus just for the conductor Y, the simulation is performed and tabled in Table 5. The Electric Field Stress of conductor Y for case 3 of GL- FGM is found in Table 5 in comparison with other GH FGM and GU FGM grades.

Table 5 - Delamination Electric Field Stress

Type	Permittivity values	Delamination Electric Field Stress at TJ without MI in KV/cm		
		V1= 72.50KV	V2=132.0 KV	V3= 220.0 KV
GL-FGM	Case1	0.160	0.29120	0.4850
	Case 2	0.1610	0.2930	0.4880
	Case 3	0.16170	0.29430	0.49040
GH-FGM	Case1	0.14760	0.26880	0.4480
	Case 2	0.14860	0.27060	0.4510
	Case 3	0.14960	0.27230	0.45380
GU-FGM	Case1	0.15020	0.27360	0.4560
	Case 2	0.150350	0.27370	0.45620
	Case 3	0.15120	0.27540	0.45890

Figure 8 shows that the magnitude of Electric field stress at the enclosure i.e. at TJ due to delamination is high, which is clearly observed that the value from Figure 9, the electric field stress at TJ is 0.1617,0.2943 and 0.4904 kV/cm at V_1= 72.5 kV, V_2=132 kV and V_3= 220KV respectively. The surface plot and the Quiver plots of the designed FGM spacers with delamination at conductor Y are as shown in figure 10 and figure 11 respectively. The red colour in both figures is representing high electric field stress at conductor V_A due to its high potential and the blue colour is indicating high electric field stress which is observed at the TJ of enclosure ends. Figure 12, figure 13 represents Quiver plot and Contour Plot of conductor Y for FGM post type spacer with delamination with high electric field stress at the Triple Junction. Similarly, the electric field stress in the designed delaminated FGM Post type spacers can be seen from the Mesh plot. The thickness or congestion of the mesh triangles is indicating that the field is high due to its curved shape as shown in figure 14 and figure 15.

Another frequent fault is metallic particles, which is causable by many procedures, leading to Spacers failure and simulating the impact of the electrical field distribution of the post-type FGM spacer with delamination and the particulate matter. The planned FGM Post type distortion with delamination and particulate matter caused significant electrical field stress at TJ at the end of container Y and so simulation for conductor Y alone is carried and is shown in Table 6. A MI is

integrated into the TJ of a box of the same conductor, as shown in figure 7, to create uniform electric field distribution across the spacer of conductor Y.

In table 6, a maximum reduction of 80.870 percent of EF stress on the TJ's of the box end is observed after MI has been inserted on conductor Y for case 3 of the GL-FGM grading of 220.0KV of operating voltage; in case 3 of GH FGM the decrease is 81.900 percent on 72.50KV and in case 3 of GU FGM the decrease is noted as 81.930 percent on the 72.50k V case 3 when the decrease is noted as 81.930 percent. Figures 16 and 17 show that the electric field stress is decreased at 72.50 kV, 132 .0KV and 200.0KV correspondingly from 0.20450 to 0.03920 k V/cm, 0.3730 to 0.07150 kV/cm and 0.6220 to 0.1190 kV/cm.

Figure 18 shows the surface graph of the FGM Delamination and Particle post-style spacer and the matching height surface graphs are as given in Figure 20. In the future, stress is reduced by utilizing the MI near TJ as illustrated in Figure 19 with the appropriate surface plots with a height after inserting the MI. The green color represents electrical field stress at Driver Y which is seen at the extremities of the container to minimize this impact at TJ Enclosure ends in Figure 19 are inserted MI's. Figures 20 and 21 show the contour plot of conductor Y to FGM post-type delaminated and high electrical field stress and MI EF stress reduction spacers, respectively. Figures 20 and 21 indicate. In the developed FGM post-type spacers, the EF stress can also be observed in the mesh plot owing to particle without and with MI. The mesh triangles are demonstrated to be of large thickness or congestion owing to their curved shape as illustrated in figures 22 and 23. The fundamental aim of the mesh plot is to define rather than a uniform color the qualities of the plot piece. Mesh plot combines diverse data sets for various plots to create the most interesting outcomes in a group of the single plot.

Fig. 8 - Effect of Delamination on FGM Post Type Spacer

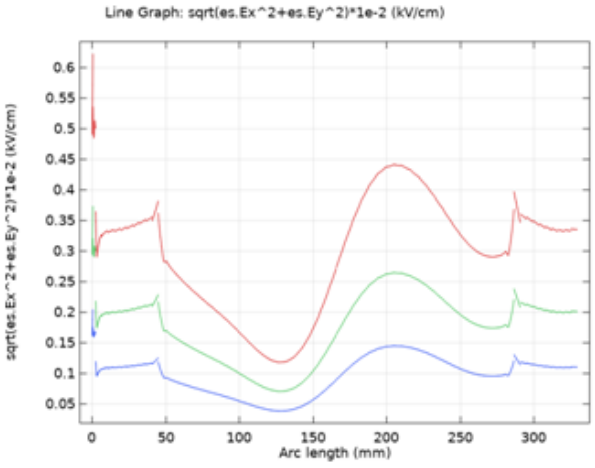

Fig. 9 - Zoomed Plot of FGM Post Type Spacer with Delamination

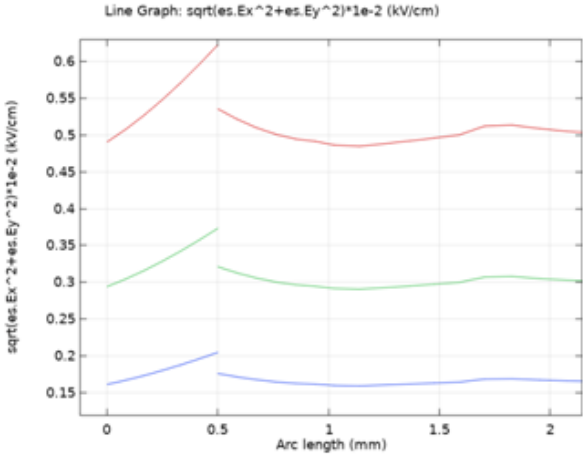

Fig. 10 - Surface Plot of FGM Post Type Spacer with Delamination

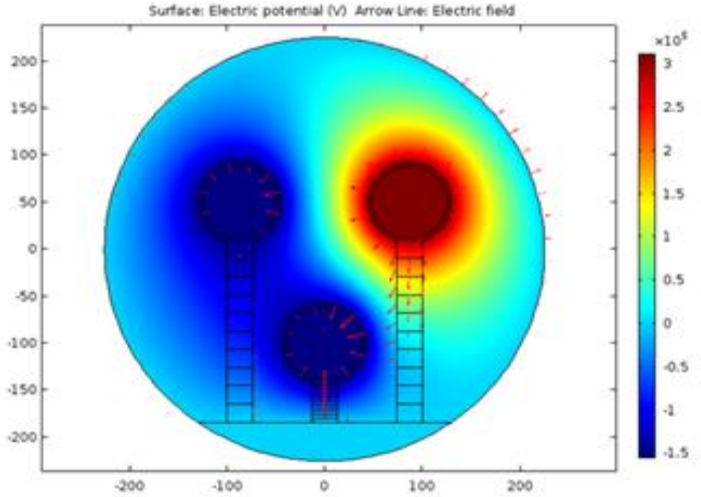

Fig. 11 - Quiver Plot- FGM Post Type Spacer with Delamination

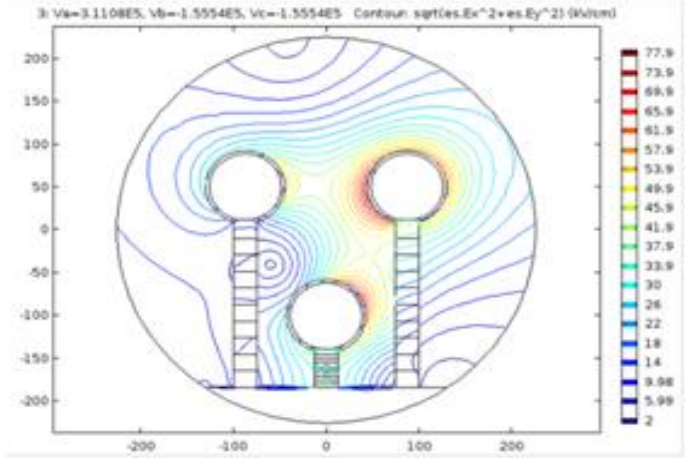

Fig. 12 - Quiver Plot- FGM Post Type Spacer with Delamination

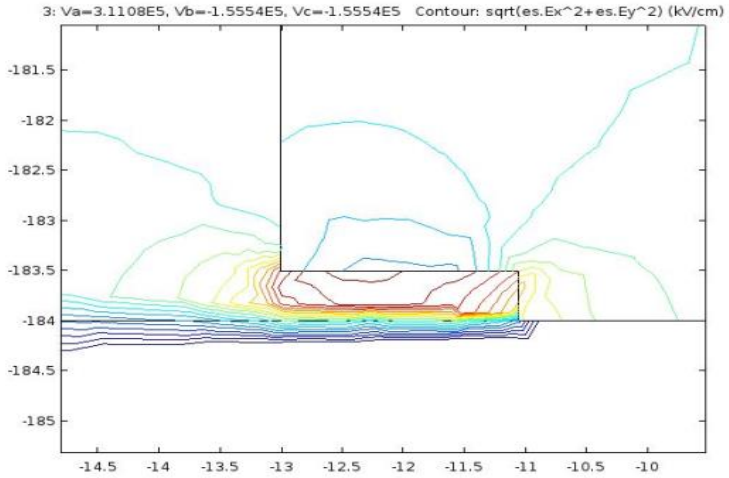

Fig.13 - Contour Plot- FGM Post type Spacer with delamination

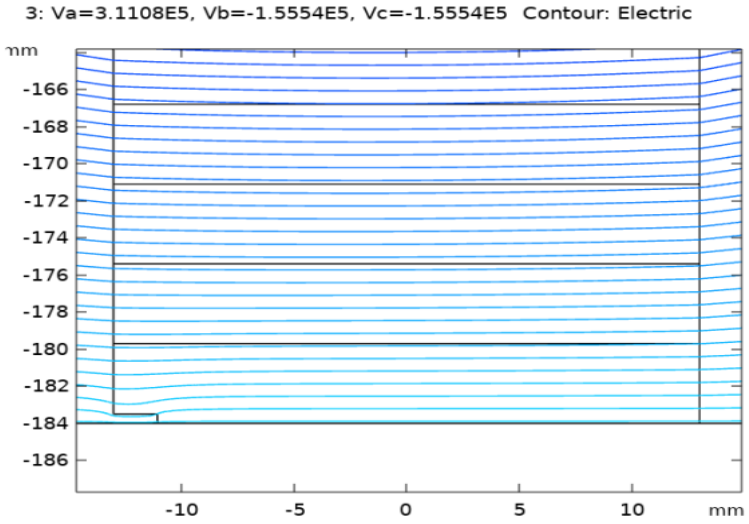

Fig. 14 - Mesh Plot of FGM Post Type Spacer with Delamination

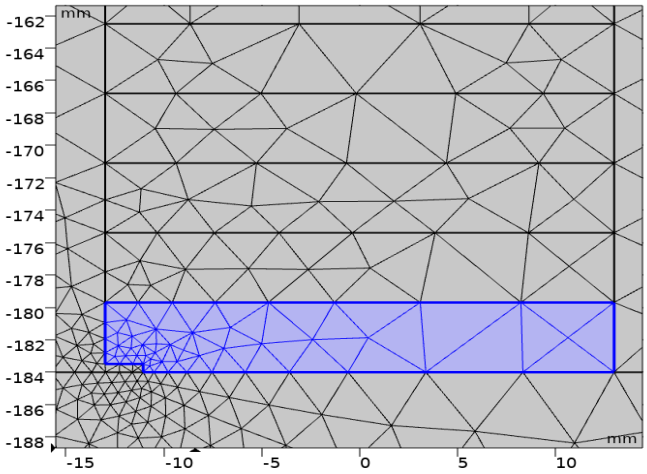

Fig. 15 - Spectrum Mesh Plot of FGM Post Type Spacer with Delamination

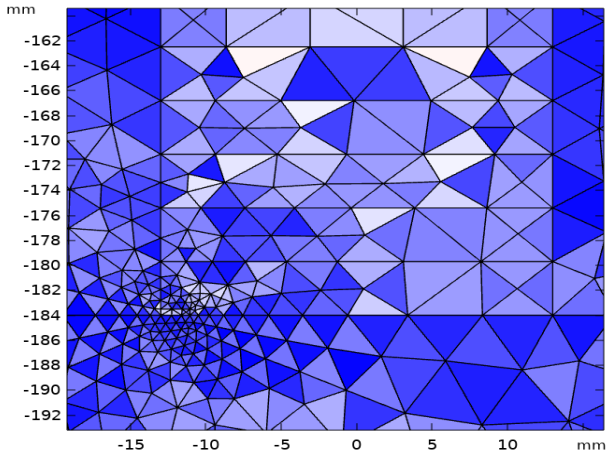

Table 6 - Delamination Electric Field Stress with Particle

Type	Permittivity	Delamination Electric field stress and Particle at TJ devoid of MI in KV/cm			Delamination Electric field stress and Particle at TJ with MI in KV/cm			% Reduction of Delamination Electric field stress and Particle at TJ due to MI		
		V_1= 72.50KV	V_2= 132.0 KV	V_3= 220.0 KV	V_1= 72.50KV	V_2= 132.0 KV	V_3= 220.0 KV	V_1= 72.50KV	V_2= 132.0 KV	V_3= 220.0 KV
GL-FGM	Case1	0.2042	0.3725	0.62	0.04023	0.0735	0.1225	80.30	80.27	80.24
	Case 2	0.2044	0.3727	0.62175	0.0397	0.0722	0.1208	80.58	80.63	80.57
	Case 3	0.2045	0.373	0.6222	0.0392	0.0715	0.119	80.83	80.83	80.87
GH-FGM	Case1	0.186	0.339	0.5654	0.0346	0.063	0.1054	81.40	81.42	81.36
	Case 2	0.1864	0.34	0.5668	0.0342	0.0624	0.1041	81.65	81.65	81.63
	Case 3	0.1867	0.3406	0.568	0.0338	0.0617	0.1029	81.90	81.88	81.88
GU-FGM	Case1	0.188	0.3427	0.5716	0.0349	0.0638	0.10645	81.44	81.38	81.38
	Case 2	0.1884	0.3435	0.5728	0.0345	0.063	0.1052	81.69	81.66	81.63
	Case 3	0.189	0.3441	0.574	0.03415	0.0623	0.104	81.93	81.89	81.88

Fig. 16 - Electric Field Characteristics of FGM Post Type Spacer which due to Delamination and Particle

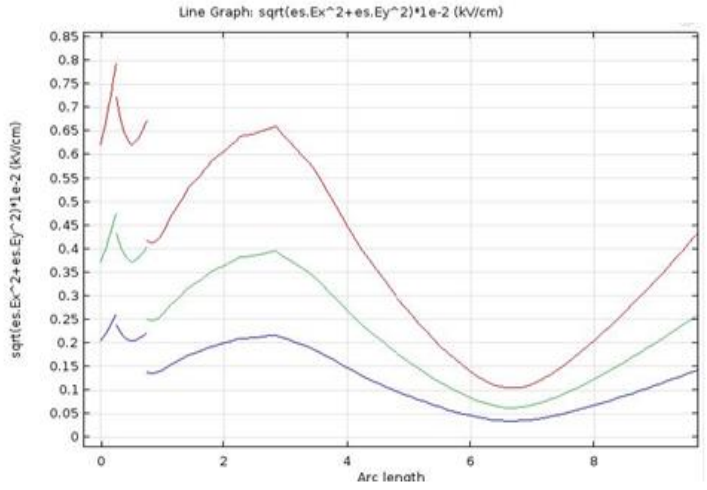

Fig. 17 - Reduced Electric Field Stress with Metal Insert at Enclosure End

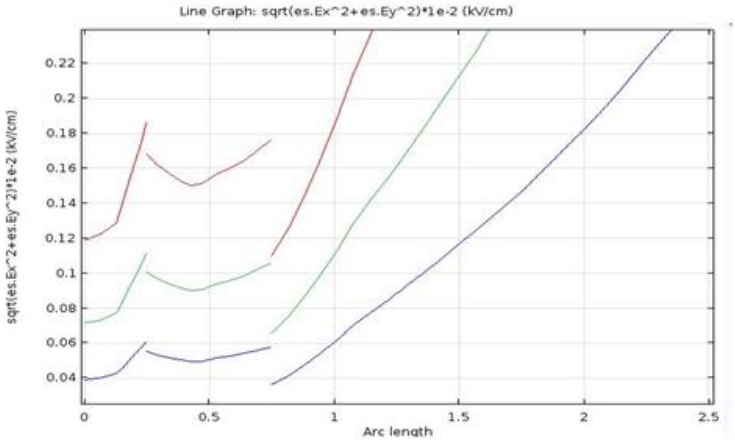

Fig. 18 - Surface Plot of FGM Post Type Spacer with Particle

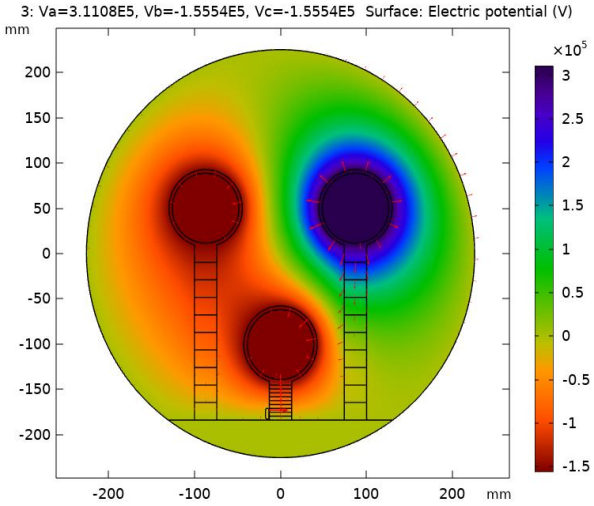

Fig. 19 - Surface Plot of FGM Post Type Spacer with Particle with Metal Insert

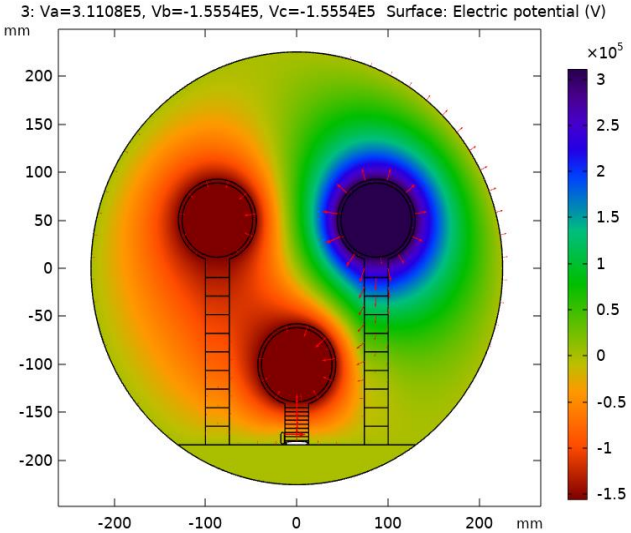

Received: 07.05.2021 – Accepted: 28.05.2021

Fig. 20 - Surface Plot with Height of FGM Post Type Spacer with Delamination and Particle

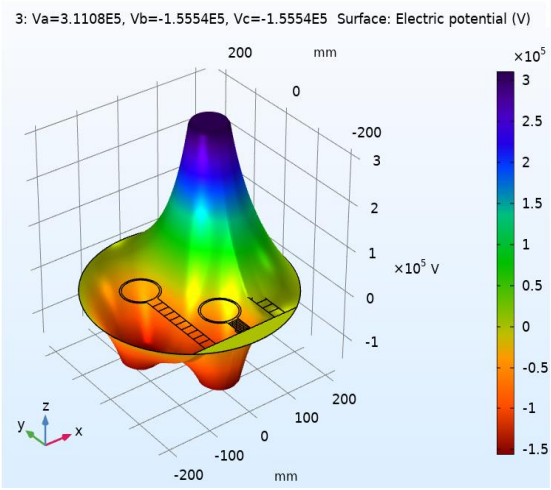

Fig. 21 - Surface Plot with Height of FGM Post type Spacer with Delamination and Particle with Metal Insert

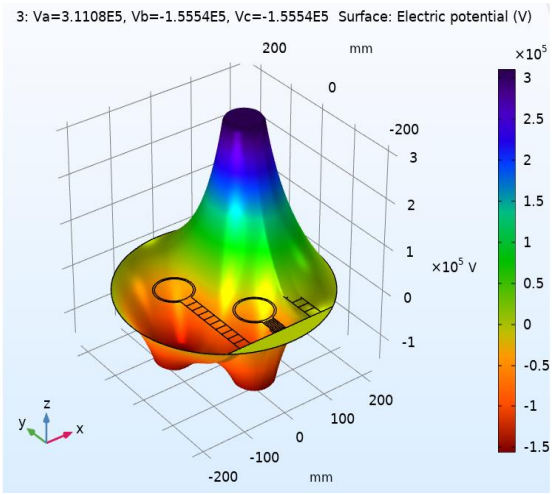

Fig. 22 - Contour Plot- FGM Post Type Spacer with Particle

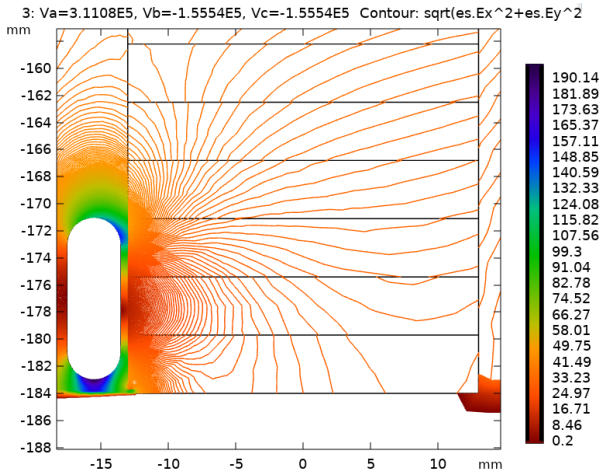

Fig. 23 - Contour Plot- FGM Post type Spacer with Particle and Metal Insert

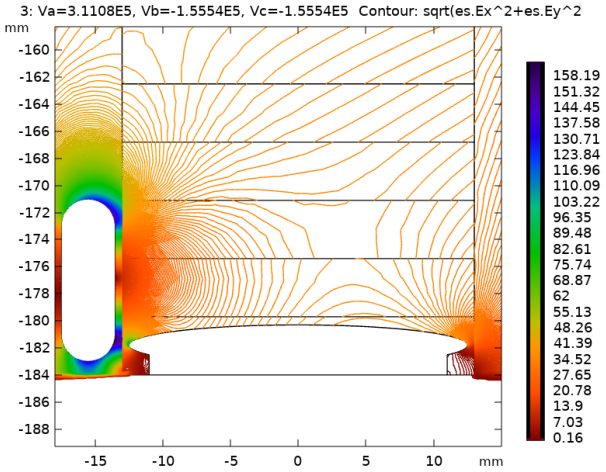

Fig. 24 - Mesh Plot of FGM Post Type Spacer with Delamination and Particle

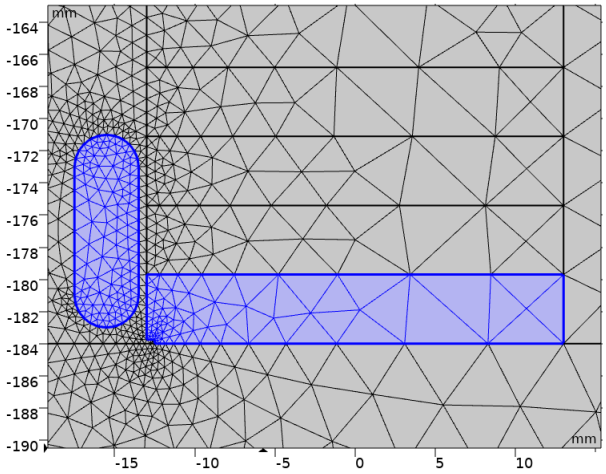

Fig. 25 - Mesh Plot of FGM Post Type Spacer with Delamination and Particle and Metal Insert

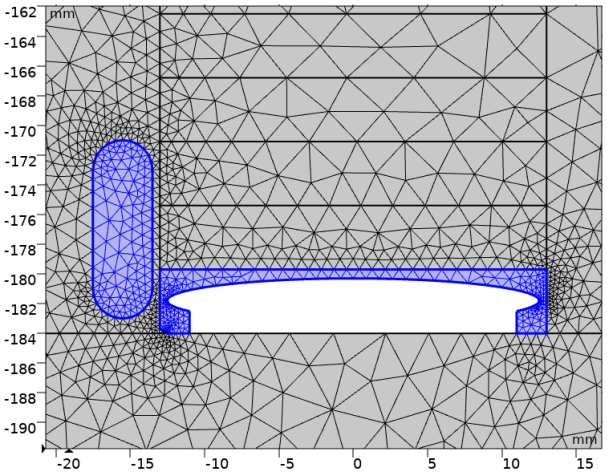

7. Conclusion

This research analyzes how important the spacer in the three phase of GIB is for the FGM postal spacer for a 3-ϕ GIB electrical fielding distribution. In order to analyze the severe defect of delamination and particulates, the three distinct types of FGM grading with various permitivity ranges are studied. It is seen that in comparison to all other conductors at different points the maximum electrical field pressure is achieved at TJ of conductor Y. Major flaws like as delamination and particulate matter are prevalent with high voltage GIB, so that different types of particles such as aluminum, copper and silver are added here. In contrast to all R, Y, and B conductors as Driver Y, TJ's enclosure end for the FGM after-type distortion has primarily high electric field stress, such that both faults are created on the same Driver Y and their influence was diminished when the MI was inserted at TJ in the space shell's end.The electronic field stress is considerable in case 3 of GL- FGM compared with other cases and GH-FGM and GU FGM ratings for fault delamination at the TJ of driver Y. The field is worsened significantly for the defect delamination alongside particle. It is observed that the high electrical field stress is achieved by the graduation of Case 3 of the GL-fGM and for Case 3 of the GU FGM by inserting a recessed metal insert in the TJ in the box end in the three-phase GIB post-grade FGM spacer.

References

Shu. Y, Chen. W, “Research and application of UHV power transmission in China”, *High Voltage,* Vol.3 (1), pp. 1-13, 2018.

Liang. H, Du. B, Li. J, Wan. Z, “Mechanical stress distribution and risk assessment of 110 kV GIS insulator considering Al2O3 settlement”, *High Voltage,* Vol.4 (1), pp. 65-71, 2019.

Talaat, M., El-Zein, A., Amin, M., “Developed optimization technique used for the distribution of U-shaped permittivity for cone type spacer in GIS”, *Electric Power Systems Research,* 163, 754-766, 2018.

Chakravorti. S, A. Lahiri, “Electrode-Spacer Contour Optimisation by ANN aided Genetic Algorithm”, *IEEE Trans. on Dielectrics and Electrical Insulation, 11*(6), 964-975, 2004.

Naidu. Y.S, Kumar. G.V.N, “Minimisation of electric field stress at triple junction of a functionally graded cone type spacer in a gas insulated busduct with metal inserts”, *High Voltage,* 2(2), 110-118, 2017.

Alan H. Cookson, “Review of high voltage gas breakdown and insulators in compressed gases”, *IEEE Proceedings on Physical Science, Meas. and Instr., Manag. and Edu.,* Vol. 128(4), 303–312, 1981.

Tanaka. H, Tanahashi. D, Baba. Y, Nagaoka. N, “Finite-difference time-domain simulation of partial discharges in a gas insulated switchgear”, *High Voltage,* Vol.1(1), 52-56, 2016.

Hong-Yang. Z, Guo-Ming. M, Wang. Y, Cheng-Rong. L, "Optical sensing in condition monitoring of gas insulated apparatus: A review", *High Voltage,* 4(4), 259-270, 2019.

Jagadeesh A, V.S.K. Rao Gadi, G.V.N. Kumar "Mitigation of field stress with metal inserts for cone type spacer in a gas insulated busduct under delamination", *Engineering Science and Technology,* 21, 850-861, 2018.

Maren Istad, Magne Runde "Thirty-Six Years of Service Experience with a National Population of Gas-Insulated Substations", *IEEE Trans. on Power Delivery*, 25(4), 2448 – 2454, 2010.

G.V.N Kumar, J. Amarnath, B.P. Singh, K.D. Srivastava, "Electric Field Effect on Metallic Particle Contamination in a Common Enclosure Gas Insulated Busduct", *IEEE Trans. on Dielec. and Elect. Insulation,* 14(2), 334-340, 2007.

G.V.N Kumar, J Amarnath, "Assessing the Risk of Failure due to Particle Contamination in GIS under various Coefficient of Restitutions", *Journal of Electrical Systems,* 10(3), 331-343, 2014.

Sun. J, Sun. L, Chen. W, Li. Z, Yan. X, Xu. Y, "Metal particle movement and distribution characteristics under AC voltage and ball-plane electrodes", *High Voltage,* 4(2), 138-143, 2019.